Self-Assembled Monolayer of Cr_7Ni Molecular Nanomagnets by Sublimation

Alberto Ghirri,[†,*] Valdis Corradini,[†] Valerio Bellini,[†] Roberto Biagi,[†,‡] Umberto del Pennino,[†,‡] Valentina De Renzi,[†,‡] Julio C. Cezar,[§] Christopher A. Muryn,[⊥] Grigore A. Timco,[⊥] Richard E. P. Winpenny,[⊥] and Marco Affronte[†,‡]

[†]S3 Centre, Institute Nanoscience—CNR, Via G. Campi 213/A, 41125 Modena (I), Italy, [‡]Dipartimento di Fisica, Università di Modena e Reggio Emilia, Via G. Campi 213/A, 41125 Modena (I), Italy, [§]European Synchrotron Radiation Facility, BP 220, F-38043 Grenoble Cédex, France, and [⊥]School of Chemistry and Photon Science Institute, University of Manchester, Oxford Road, Manchester, M13 9PL, U.K.

ABSTRACT We show, by complementary spectroscopic and STM analysis, that Cr_7Ni derivatives are suitable to be sublimed in UHV conditions. Cr_7Ni-*bu* weakly bonds to gold surface and can diffuse relatively freely on it, forming monolayers with hexagonal 2D packing. Conversely, by adding a functional *thiol* group to the central dibutylamine, a covalent bond between the molecule and surface gold adatoms is promoted, leading to a strong molecular grafting and the formation of a disordered monolayer. These two examples demonstrate the possibility to control the assembly of a large molecular complex, as rationalized by DFT calculations that establish different energy scales in the deposition processes. Moreover, low-temperature XMCD sprectra show that the magnetic features of Cr_7Ni rings deposited in UHV on gold remain unchanged with respect to those of the corresponding bulk sample.

KEYWORDS: molecular magnets · self-assembly · thermal deposition · thiol · STM · XMCD · density functional theory

The control of molecular assembly on surfaces provides a very efficient method for the realization of ordered arrays of molecular objects,[1] an important issue toward applications in nanotechnologies.[2,3] Molecular self-assembly on surfaces has indeed attracted wide interest in the last decades. From simple organic molecules[4,5] to more complex phthalocyanines,[6] porphyrines,[7] and bis(phthalocyaninato) rare earth complexes[8,9] many beautiful examples of surfaces decorated with molecules in complex architectures have been documented.[10] In general terms, the assembly is determined by the interplay between molecule–substrate and molecule–molecule interactions. For instance, by introducing selected end-groups, it is possible to modulate the bonding with the substrate.[7,11] In the limit of molecules free to diffuse on the surface, they will tend to self-organize driven by the sole molecule–molecule interaction.

While there is extensive literature on simple molecules, self-assembly of large complexes is much less documented, due, in part, to the fragile nature of large molecules and to the insufficient control in the driving mechanism of their assembly on surfaces. The interest here is especially devoted to presynthesized aggregates that show specific functions at the single-molecule level. Among these, molecular nanomagnets (MnM) are prominent examples, in which intriguing classical or quantum effects occur.[12] For instance, genuine quantum phenomena, such as mixing of different spin states[13] and coherent spin dynamics,[14] have been experimentally observed on antiferromagnetic rings of Cr_7Ni, and this led to proposing them as molecular *qubits* for the implementation of quantum information processing.[15] Moreover, the possibility to engineer supramolecular complexes with linked magnetic states has been demonstrated, along with spin entanglement at the supramolecular level.[16–18]

Initially, the functionalization of either MnM or the surface with deposition from the liquid phase was chosen,[19,20] and the successful decoration of gold,[21–24] silicon,[25] and graphite[26] surfaces has been largely documented. The implicit choice here is to firmly graft molecules on a substrate. The integrity of the molecules, as well as the essential preservation of their magnetic properties at the surface, has been largely debated, and finally it was demonstrated for selected derivatives of Fe_4[27] and Cr_7Ni[28] nanomagnets. Despite these successes, liquid-phase deposition faces intrinsic limitations, due to the presence of solvent residuals, contaminant species, and the difficulty to control the distribution and coverage of the adsorbates. Moreover, high-vacuum deposition methods are required for preparing cleaner and more controlled interfaces suitable for in-depth investigations of the structural, electronic, and magnetic properties, such as

* Address correspondence to alberto.ghirri@nano.cnr.it.

Received for review May 17, 2011 and accepted August 2, 2011.

Published online August 02, 2011
10.1021/nn201800e

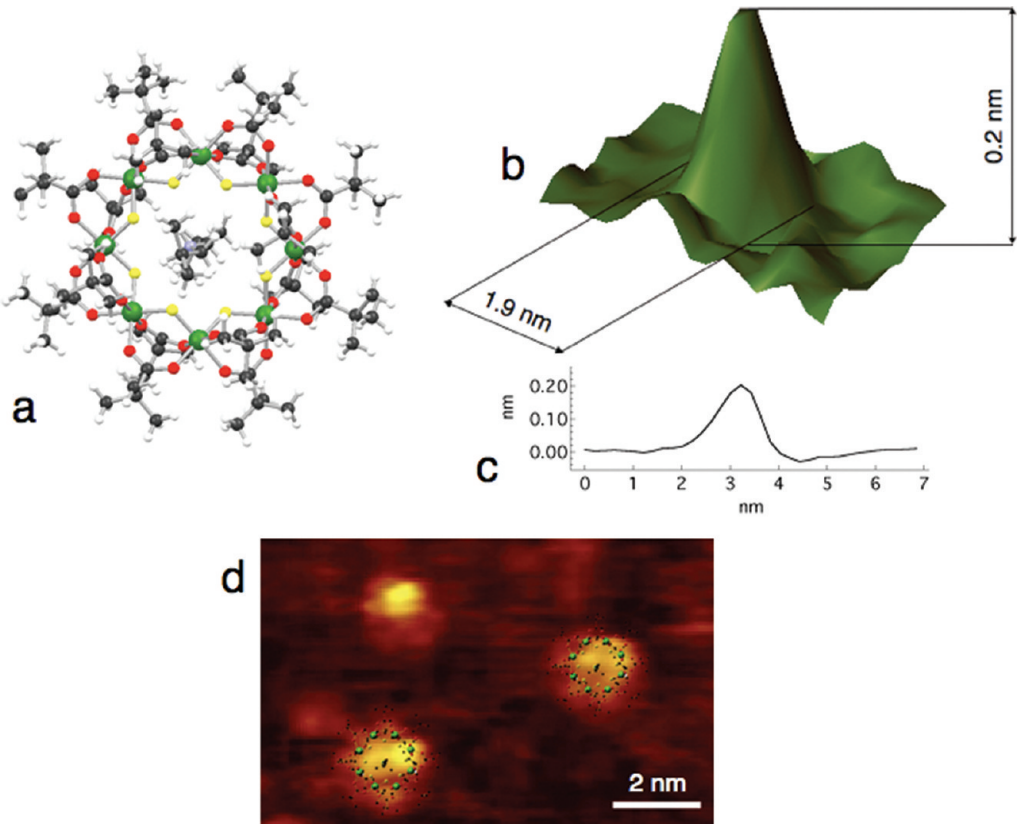

Figure 1. (a) Crystallographic structure of the Cr_7Ni-*bu* molecule (top view). Colors: C, black; H, white; O, red; F, yellow; N, cyan; Cr and Ni, green. (b) STM image and (c) profile of an isolated Cr_7Ni-*bu* on Au(111) (tunneling conditions: 2 V and 20 pA). (d) STM image of Cr_7Ni-*thiobu* on Cu(110) (tunneling conditions: 2 V and 500 pA).

valence-band, energy-loss, and X-ray diffraction spectroscopies and low-temperature scanning tunneling microscopy (STM) and spectroscopy (STS). For these experiments, vapor deposition in ultrahigh vacuum (UHV) guarantees the cleanest conditions, provided that molecules are strong enough to withstand the thermal degradation. Powder samples of MnM must be heated to a few hundreds of degrees Celsius before the sublimation occurs. Therefore, so far the thermal deposition of molecular magnets has been reported only in a few cases.[29−32] A soft deposition method compatible with UHV conditions is electrospray, which can be successfully applied to soft molecules as well to MnM.[33,34]

An alternative approach is to leave nonfunctionalized molecules relatively free *to float on a 2D pool*.[35] The organization of molecules deposited onto surfaces is governed by the interplay between deposition flux and diffusion rate.[1] Typically, the van der Waals (vdW) interaction is always present and sufficient to stick molecules on a surface while they are still free to pack in ordered arrays. This approach is certainly preferable to obtain a large (and complete) coverage of MnM on surfaces.

Here we report on the vapor deposition of two derivatives of Cr_7Ni rings, namely, $\{[(CH_3)_2CHCH_2]_2NH_2\}\{Cr_7NiF_8[O_2CC(CH_3)_3]_{16}\}$, in short Cr_7Ni-*bu*, and $\{HSCH_2CH_2NH_2CH_2CH_2CH_2CH_3\}\{Cr_7NiF_8[O_2CC(CH_3)_3]_{16}\}$, in short Cr_7Ni-*thiobu*, and their assembly on the Au(111) surface. Both clusters have identical magnetic cores and peripheral pivalic groups, while Cr_7Ni-*thiobu* rings differ from the pristine Cr_7Ni-*bu* derivative solely in the substitution of the central diisobutylamine with the 2-(butylamino-)ethanethiol. By exploiting the high affinity between S and Au, the thiol functional group establishes a covalent bond between the molecule and the gold surface.[36] This substitution gives significant differences in the assembly of Cr_7Ni-*bu* and Cr_7Ni-*thiobu* on Au(111). We start by showing that both derivatives are stable upon heating and thus suitable for deposition by sublimation; then we report on their organization on the gold surface, and we discuss this within the framework of first-principles calculations. Finally, by means of X-ray adsorption spectroscopy (XAS) and X-ray magnetic circular dichrosim (XMCD) we show the full retention of the molecule electronic and magnetic properties in the case of the Cr_7Ni-*bu* derivative.

RESULTS

Ultrahigh Vacuum Sublimation of Cr_7Ni Rings. The deposition of Cr_7Ni-*bu* and Cr_7Ni-*thiobu* rings on a Au(111) surface was carried out by sublimation of dry microcrystalline powders in ultrahigh vacuum (see Methods section for details). A preliminary test of the stability of Cr_7Ni molecules was performed by thermal gravimetric

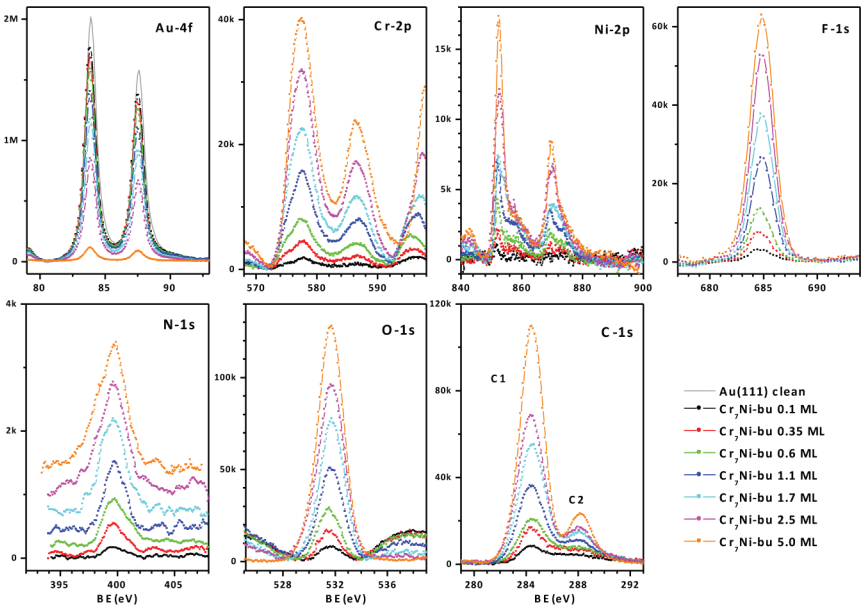

Figure 2. XPS core level spectra of the Cr_7Ni-*bu* deposited on a Au(111) surface by sublimation at 200 °C for the different coverages.

analysis (TGA). From the measured thermograms (heating rate 5 °C/min in N_2 flow 100 cm^3/min) we observed that Cr_7Ni-*bu* and Cr_7Ni-*thiobu* start to sublimate at about 180 °C, and a negligible weight loss (<0.3%) is detectable up to 295 °C. This result is in line with what was already obtained for other volatile clusters comprising pivalic groups.[29,37] To further check the thermal stability of these Cr_7Ni derivatives, we measured the infrared spectra of baked powders (230 °C) and thick films sublimated on KBr pellets at 230 °C and compared the results with those of the pristine powders (see Supporting Information (SI)). The remarkable correspondence of peak positions and relative intensity clearly shows that the vibrational properties of the molecules are preserved after the sublimation process. The sublimates were also checked by electrospray mass spectrometry. Both Cr_7Ni-*bu* and Cr_7Ni-*thiobu* compounds show the same mass spectrum as before sublimation.

The intact vacuum sublimation of the MnM has also been confirmed by the formation of single crystals used for diffraction measurements (see SI). The resulting diffraction patterns can be solved and yield structures with complete wheels and central amine groups, indicating that the molecules are stable with respect to sublimation (Figure 1a). A systematic investigation of a range of wheels and horseshoes and their sublimation capability will be described in a forthcoming publication that demonstrates the general validity of the results reported here. In nearly all cases the bare eight-metal wheels have been found to sublime intact, while the presence of terminal groups replacing the pivalate or the central amine group can significantly affect the sublimation capability. Trimethylacetic acid (pivalic acid (HPiv)) is more suitable for obtaining volatile compounds. It contains the *tert*-butyl group, which has a large volume and creates steric hindrances that reduce the intermolecular interaction in the solid state. In our opinion this might be the reason for the relatively high volatilities of metal pivalates.[37]

Magnetic susceptibility measurements on baked powders show the usual behavior of the pristine derivative. We just mention that isolated Cr_7Ni-*bu* molecules deposited from liquid phase show a weak interaction with the gold surface that only slightly alters their low-energy pattern of magnetic states.[24,28]

Further evidence of the integrity of the molecules is given by STM and X-ray photoemission spectroscopy (XPS) analysis. For short deposition times, regular spots are visible on the gold surface by STM (Figure 1b and d), and they can be reasonably attributed to isolated Cr_7Ni molecules. Line profiles (Figure 1c) of these spots give indeed a lateral size of 1.9 $\pm$ 0.2 nm, a value that perfectly matches the crystallographic diameter of the Cr_7Ni-*bu* molecule (1.9 nm) estimated by X-ray diffraction[38] (Figure 1a). The apparent height of the Cr_7Ni-*bu* molecules (0.20 $\pm$ 0.05 nm) is lower than the hard sphere dimension (1.1 nm), but this is due to a lower local density of states associated with the molecules as compared with the metallic Au surface, as discussed in the literature.[33] These results further corroborate the integrity of the molecules after sublimation and deposition. Moreover, the ratio between height and lateral size measured by STM indicates that molecular Cr_7Ni rings lay flat on the gold (or copper) surface. This is the most favorable configuration that maximizes the contact surface between such flat Cr_7Ni molecules and the substrate, as confirmed by calculations presented in the following.

TABLE 1. Stoichiometric Values Derived from the Core Level Intensities of the Cr_7Ni-*bu* and Cr_7Ni-*thiobu* Rings Deposited by Sublimation on the Au(111) Surface[a]

derivative	Cr-2p/Ni-2p [7.0]	F-1s/Cr-2p [1.14]	N-1s/7Cr-2p [1]	S-2p/7Cr-2p [1]	O-1s/7Cr-2p [32]	C-1s/7Cr-2p
Cr_7Ni-*bu*	7.2 ± 0.5	1.17 ± 0.05	1.10 ± 0.15		29 ± 5	90 ± 15 [88]
Cr_7Ni-*thiobu*	6.8 ± 0.5	1.13 ± 0.05	0.90 ± 0.15	1.00 ± 0.15	30 ± 5	95 ± 15 [86]

[a] The expected stoichiometric values are reported in brackets.

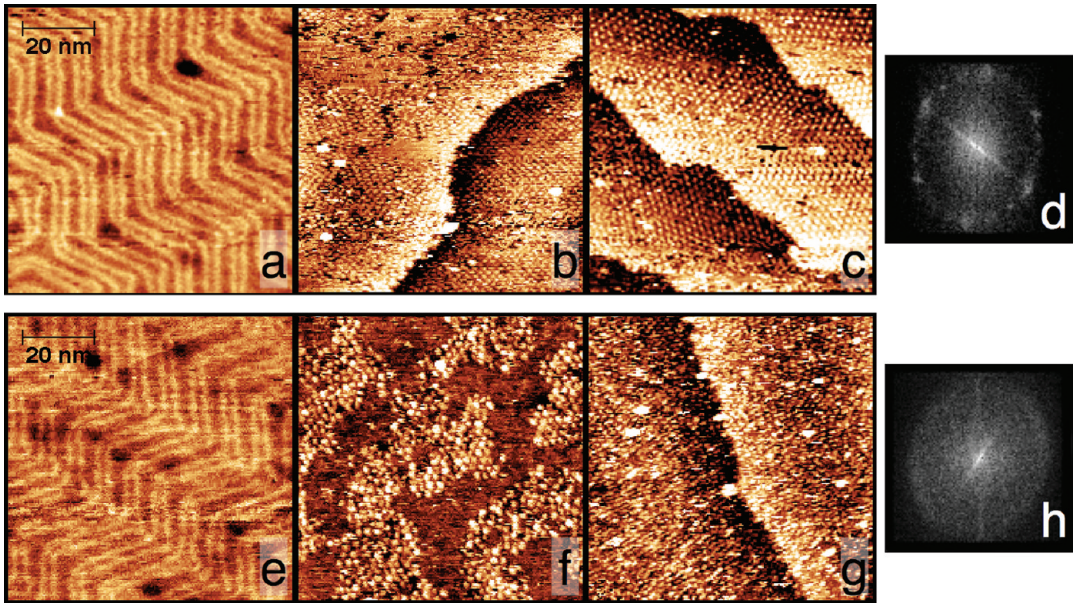

Figure 3. (a–c) STM images showing sequential steps of the vapor deposition of Cr_7Ni-*bu*: (a) clean Au(111) surface; (b) half a monolayer of Cr_7Ni-*bu* molecules; (c) complete self-assembled monolayer. (d) Fourier transform of the STM image showing hexagonal symmetry. (e–g) STM images showing sequential steps of the vapor deposition of Cr_7Ni-*thiobu*: (e) clean Au(111) surface; (f) half a monolayer of Cr_7Ni-*thiobu* molecules that follow the underlying herringbone modulation of the Au(111) surface; (g) complete monolayer of Cr_7Ni-*thiobu* molecules with some 3D aggregates. (h) Fourier transform of the STM image showing no particular ordering. Tunneling conditions: 2 V and 20 pA. Scan area 76 × 76 nm^2.

By means of XPS, we have investigated in detail the chemical composition of the Cr_7Ni-*bu* molecules deposited on a Au(111) surface in UHV conditions. In Figure 2 the core levels of the Cr_7Ni-*bu*/Au(111) interface deposited by sublimation at 200 °C are shown for the different coverages. Core level intensities have been analyzed taking into account the atomic sensitivity and the attenuation of the electronic signals. The Cr 2p, F 1s, Ni 2p, and N 1s core level line shapes measured for all the depositions fit well with the corresponding data obtained on a Cr_7Ni-*bu* thick film deposited from the liquid phase.[24,39] The stoichiometric ratios are well reproducible and close to the expected ones (see Table 1), clearly indicating that the overall molecular stoichiometry is preserved during the heating and deposition processes. More in detail, in the C-1s core level spectra two components are evident, C_1 at 284.5 eV (typical of hydrocarbons) and C_2 at 288.3 eV (due to carboxylates). In the Cr_7Ni-*bu* rings under study, there are 16 carbons in the carboxylates and 72 in the diisobutylamine and methyl groups. The fact that the C_1 component is 4.5 ± 1.0 times higher than C_2 (in agreement with the expected ratio of 4.5) indicates not only that the stoichiometry is preserved but also that the carboxylate bridges are unaffected. The preservation of the N-1s/7Cr-2p ratio confirms that the amine placed at the center of each Cr_7Ni ring is stable too.

From the Au-4f/Cr-2p ratio and by taking into account the Au signal attenuation due to the overlayer, we obtained the average area occupied by one Cr_7Ni ring for the different deposition times. Assuming that the complete coverage is made by molecules lying flat on the surface and considering an area of 2.8 nm^2 for each molecule, we derived the thickness of the Cr_7Ni-*bu* film for the different deposition times (see Figure S3 in SI). Just to fix some numbers, it turns out that in our setup when powders are heated at $T_h \simeq 200$ °C (230 °C), the time required to obtain one monolayer is about 120 min (20 min).

Assembly of Monolayers. The organization of Cr_7Ni-*bu* on Au(111) was first investigated by means of STM. As a preliminary step, we prepared a clean Au(111) surface on which the $22\times\sqrt{3}$ "*herringbone*" reconstruction was clearly visible (Figure 3a). For a crucible temperature of $T_h \simeq 200$ °C, STM images show the beginning of

deposition after a few minutes, in agreement with the XPS results (Figure 2). The coverage progressively increases with deposition time. Figure 3b shows the surface covered by about half a monolayer of molecules, which start to assemble in planar layers with no indication of 3D aggregation. Molecular assemblies nucleate with hexagonal symmetry and regular separation between spots (pitch) of 2.1 ± 0.2 nm. By increasing the exposure time, the formation of a complete self-assembled monolayer was observed (Figure 3c). Here, the Cr_7Ni-*bu* molecules clearly give shape to an extended ordered lattice. Fourier transform of the STM image gives the hexagonal-centered pattern shown in Figure 3d. Careful analysis of the STM images also shows the presence of a texture with different domains slightly misaligned from each other. They are extended over hundreds of nanometers, covering the whole surface of the gold single crystal. Interestingly, the hexagonal lattice of nonfunctionalized Cr_7Ni-*bu* molecules is incommensurate with the underlying Au(111) surface, and, more specifically, no particular matching with the herringbone reconstruction was found.

Scanning parameters of the STM measurements give qualitative information on the molecule−surface interaction as discussed in detail in the SI. Briefly, our findings indicate that Cr_7Ni-*bu* molecules are relatively free to move on the gold surface while they tend to closely pack together.

To control the interaction between molecules and the gold surface, trying to anchor the molecular Cr_7Ni rings more tightly to the surface, the (butylamino)ethanethiol group was added to the molecule, giving the Cr_7Ni-*thiobu* derivative. The integrity of this functionalized derivative upon sublimation, as previously described, was preliminarily checked. Briefly, the core levels of the Cr_7Ni-*thiobu* (see SI) deposited on the Au(111) surface by sublimation ($T_h \simeq 185$ °C) perfectly match those of the Cr_7Ni-*bu* reported in Figure 2. We chose $T_h \simeq 185$ °C in order to have, for the two derivatives, the same growth rate of 1 monolayer (ML) in 120 min of exposure. Also for Cr_7Ni-*thiobu* the stoichiometric ratios are well reproducible and close to the expected ones (Table 1), clearly indicating that the ring stoichiometry is preserved also in this case. In particular, the N-1s/7Cr-2p and S-2p/7Cr-2p ratios are retained, confirming the stability of the 2-(butylamino)ethanethiol ligand.

Figure 3e−g shows STM images of the Cr_7Ni-*thiobu* deposited on the Au(111) surface. For low coverages, the molecules form flat 2D aggregates and somehow tend to follow the herringbone pattern on the Au(111) surface (Figure 3f). The first layer is formed with no evidence of large-scale ordering, and few random 3D aggregates are visible (Figure 3g). The Fourier transform of such an image is indeed a circular halo (Figure 3h), confirming the lack of ordering.

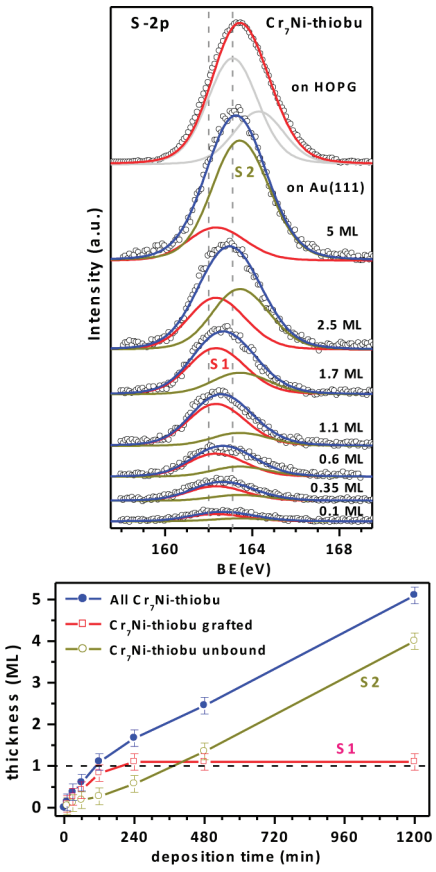

Figure 4. S-2p core level fits for the different coverages of the Cr_7Ni-*thiobu* deposited by sublimation on the Au(111) and HOPG surfaces. The best-fit parameters for the S_1 and S_2 components are reported in the text. Bottom panel: thickness *vs* deposition times for the Cr_7Ni-*thiobu* with the thiol bound to gold (open squares) derived by the S_1 component, the Cr_7Ni-*thiobu* with an unbound thiol (open circles) derived by S_2, and their sum (filled circles). The coverage of the grafted-Cr_7Ni saturates at about 1 ML.

Quantitative XPS analysis of sulfur (S) core levels allowed us to monitor the effectiveness of the anchoring of the *thiol* group on the gold surface. Two S-2p components are observed at 162.0 eV (S_1) and 163.1 eV (S_2) (Figure 4). S_1 can be assigned to S atoms bonded to gold, while S_2 to unbound S atoms,[40−42] due to the presence of a second layer of Cr_7Ni-*thiobu* molecules. To clarify this point, the spectrum of the Cr_7Ni-*thiobu* deposited in the same way on the HOPG surface (on which only unbound S is expected) is also plotted in Figure 4: actually only peak S_2 at 163.1 eV is present in this case. From the Au-4f/S_1 and Au-4f/S_2 ratios, we derived the thickness of the Cr_7Ni-*thiobu* layers with (i) the thiol bound to gold (grafted Cr_7Ni), (ii) unbound thiol (unbound Cr_7Ni), and (iii) the overall Cr_7Ni-*thiobu* coverage (Figure 4 bottom panel) assuming that the complete coverage is made by molecules lying flat on the surface (area of 2.8 nm^2). At low coverage, 4/5 of the deposited rings are grafted. This means that after 120 min, when 1 ML of molecules has been deposited, 80% of the surface is covered by a first layer of grafted

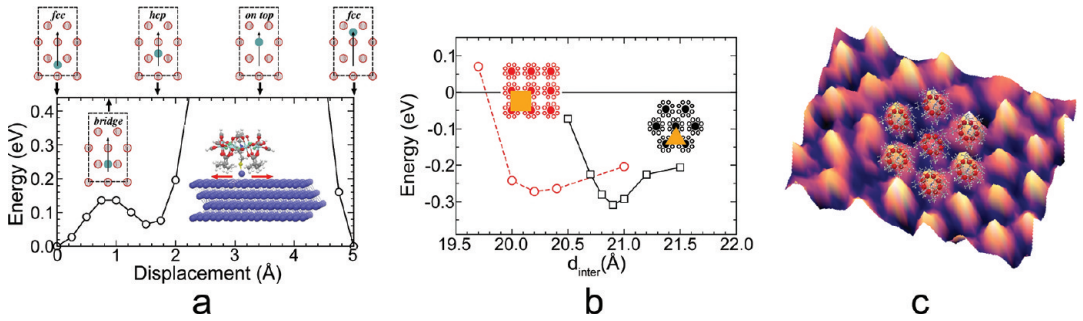

Figure 5. (a) Energy barrier felt by the Cr_7Ni-*thiobu* as a function of the displacement across the Au(111) substrate; the displacement line has been chosen to span different adsorption/symmetry sites for the Au adatom. (b) Interaction energy/molecule in the case of a square or hexagonal arrangement of the Cr_7Ni-*bu* molecules as a function of the molecule−molecule distance. (c) High-resolution STM images (zoom of Figure 3c), with, superimposed to it, the DFT-predicted structure.

Cr_7Ni and 20% by a second layer of unbound Cr_7Ni, in agreement with STM images in Figure 3g. The S_1 component saturates (*i.e.*, the first layer of grafted Cr_7Ni has been completed) after 240 min (1.7 ML), while for longer deposition time only the S_2 signal still increases (Figure 4). It is interesting to note that the ratio Au-4f/S_1 does not show any excess of thiols, in contrast to the liquid-phase deposition of Cr_7Ni-*thiobu*/Au(111), where the partial instability of the (butylamino)-ethanethiol group was observed.[24,39] These results clearly demonstrate the effectiveness of the S−Au bond and, consequently, the different mechanism of grafting and assembly of functionalized Cr_7Ni-*thiobu* rings.

As a complementary experiment we also investigated by STM the organization of Cr_7Ni-*thiobu* molecules sublimated onto Cu(110). The bonding of sulfur on copper is expected to be strong, too, and to give results similar to the ones obtained on Au(111). Here the molecules show no ordering, as the molecule−surface interaction dominates the much weaker molecule−molecule interaction. The high stability of the molecules on the copper surface is further proved by the ability to image the molecules at high tunneling currents of up to 0.5 nA, with a range of voltages up to 2 V. This causes no change to the molecules on the surface. The increased tunneling current that can be employed allowed imaging the molecules with higher spatial resolution, a result really difficult to achieve with the low currents needed for the gold surface. This is clearly evident in Figure 1d, in which lobes around the center of the molecule are seen and there is clear topographical structure associated with the molecule. This can in simplistic terms be interpreted by overlaying the scaled structure of the molecule on the STM image.

Modeling. The different behavior of Cr_7Ni-*bu vs* Cr_7Ni-*thiobu* rings can be explained by the following rationale. The Cr_7Ni-*bu*−Au(111) interaction energy is smaller than the Cr_7Ni-*thiobu*−Au(111) one. Moreover, Cr_7Ni-*bu* molecules can move—relatively free of lateral constraints—on the Au(111) surface, while Cr_7Ni-*thiobu* experiences some kind of corrugation potential from the Au(111) (and Cu(110)) surface and is less mobile. The interaction among Cr_7Ni-*bu* molecules is rather isotropic, so that they minimize the energy of the system by assembling themselves with the densest possible packing, *i.e.*, the hexagonal one. In order to endorse the above assertions, a density functional first-principles characterization of the molecule−surface and molecule−molecule interactions was undertaken.

Molecule−Surface Interaction. Cr_7Ni-*bu* interacts mainly by van der Waals forces acting between the atoms of the pivalic (*piv*) groups and the Au ones. Cr_7Ni-*thiobu*, as demonstrated in the experiments, interacts also by covalently bonding the S atoms of the thiol with Au atoms of the substrate, after dehydrogenation of the S−H bond. In an undistorted molecule lying on a flat Au(111) surface (see Figure 5a), due to the protruding pivalic groups, the S−Au distance would be too large for covalent bonding. Nevertheless, it is well known in the literature that deconstruction of the compressed herringbone structure of clean Au(111) often occurs upon molecular adsorption and determines the presence of adatoms diffusing on the surface.[43,44] Indeed, the role of adatoms on the structure and formation of a thiol-based self-assembled monolayer have been recently largely discussed in the literature.[36,45] In the presence of adatoms on the surface the S−Au-adatom distance allows the formation of a covalent bond. The molecular grafting through S−Au-adatom bonding has been theoretically investigated, finding that the most likely configuration is with Au on a *fcc* stacking position (Figure 5a).

Performing electronic and structural minimization with the molecules, either grafted on the surface or placed far away from it (15 Å), the adsorption energy, E_{ads}, was obtained as the total energy difference between the two configurations. The Cr_7Ni-*thiobu* ring is found to firmly graft on the Au substrate, thanks to the S−Au covalent bond, but it is worth stressing that a pure vdW interaction is also able to provide robust grafting of the Cr_7Ni-*bu* molecules, the two adsorption energies being ΔE_{abs}^{thiobu} =4.5 eV and ΔE_{abs}^{bu} = 2.6 eV, respectively. The calculated equilibrium distances between the lower H atoms of the *piv* groups and the Au

surface atoms are 2.3 Å in the case of Cr_7Ni-*bu* and 2.7 Å in the case of Cr_7Ni-*thiobu*. From the analysis of the energy curve *vs* molecule−surface distance (by imposing a 2.7 Å distance in the Cr_7Ni-*bu*−Au(111) interface) it turns out that about half of the adsorption energy of Cr_7Ni-*thiobu* is given by vdW interactions and the rest by the covalent bond's formation.

Next we focus on the energy barriers that the molecule faces when diffusing across the Au surface and investigate how the total energy of the system is altered when the molecules are rigidly translated across the surface. In the case of Cr_7Ni-*thiobu*, the translation line has been chosen such that it spans the possible symmetry position (*fcc*, *hcp*, *bridge*, and *on-top*) of the Au adatom (see insets in Figure 5a). We further assume that the Au adatom is displaced rigidly with the molecule (see also SI for a more in-depth discussion). The result of such calculations is shown in Figure 5a. The behavior is, as expected, similar to that of the surface energy of a free Au atom as it spans the same symmetry points. The Cr_7Ni-*thiobu* molecule is faced with an energy barrier of around 0.15 eV when moving its anchoring point from a *fcc* to a *hcp* site crossing a *bridge* site. In similar numerical simulations, Cr_7Ni-*bu* is shifted along the same line, although no clear binding site could be defined in this case. The total energy shows variations on the order of 0.005 eV or less (not shown); thus this derivative does not experience the periodicity of the atomic Au network below and Cr_7Ni-*bu* are basically free to "float on the Au(111) pool" (surface). A similar behavior has been already reported for the case of planar molecules on Au(111).[35]

On the contrary, Cr_7Ni-*thiobu* molecules feel also an in-plane corrugation potential, due to the covalent interaction with Au (Cu) adatoms, and have to overcome the energy barriers shown in Figure 5a. These findings well explain our experimental STM observations showing that Cr_7Ni-*thiobu* is more stable than Cr_7Ni-*bu* upon repeated scanning of Au(111) and further corroborated by the behavior observed on Cu(110).

Molecule−Molecule Interaction. The explanation of the hexagonal packing should thus not be sought in a surface-driven assembly, but derives from the type of intermolecular interactions acting between the molecules within the monolayer plane. We considered the vdW interaction between two Cr_7Ni molecules in the absence of the Au substrate as a function of the distance and relative orientations, representative of the situation where one (or two) *piv* group of one molecule is facing either one or two *piv* groups of the neighbor molecule, and as a function of the distance between the two ring centers. The optimal intermolecular distance, d_{inter}, is found to vary between around 2.0 and 2.1 nm, in excellent agreement with experiments, as the number of *piv* groups facing each other decreases (see SI). The size of the vdW interaction between the molecules is found to be 1 order of magnitude smaller than the molecule−surface one, while it is the same size as the corrugation energy felt during lateral displacements of the Cr_7Ni-*thiobu* molecule depicted in Figure 5a. Then the interaction energy of an array of molecules supposing either a two-dimensional square or hexagonal periodic packing was calculated (again without considering the Au substrate below). Figure 5b shows the attractive energy/molecule (the zero energy is relative to the molecules set at a large distance from each other, ∼30 Å). Although square packing would allow the molecules to be closer to each other, it is evident that hexagonal packing is energetically favored (0.04 eV/molecule). These results are summarized in Figure 5c, where the theoretical packing predicted by density functional theory (DFT) calculations is superimposed on a high-resolution STM image obtained for the Cr_7Ni-*bu* molecule: the agreement between model and experiments is excellent.

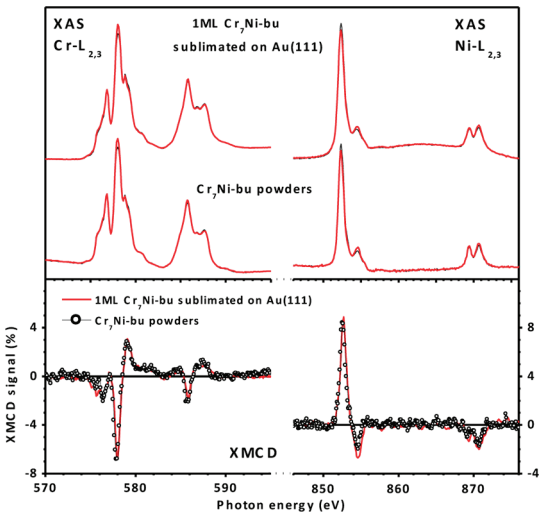

Figure 6. Upper panel: Cr and Ni $L_{2,3}$ XAS spectra taken with $\sigma^{\uparrow\uparrow}$ (thick lines) and $\sigma^{\uparrow\downarrow}$ (thin lines) circularly polarized light at 5 T and 7 K for one ML of Cr_7Ni-*bu* deposited by sublimation on Au(111) and the Cr_7Ni-*bu* powders. Lower panel: Comparison between the corresponding XMCD ($\sigma^{\uparrow\downarrow}-\sigma^{\uparrow\uparrow}$) spectra.

Low-Temperature XAS and XMCD Measurements. To check the chemical, electronic, and magnetic properties of the Cr_7Ni rings deposited in UHV, data from low-temperature spectroscopic techniques are reported and discussed in this section. In Figure 6 the Cr and Ni $L_{2,3}$ XAS and XMCD spectra (measured at 5 T and 7 K) of one ML of Cr_7Ni-*bu* sublimated on the Au(111) surface are compared with the corresponding powders. The XAS and XMCD spectral line shapes practically overlap each other. The Cr absorption spectra present eight features characteristic of Cr^{3+} in an O_h environment, whereas Ni presents two peaks at the L_3 edge and a partially resolved doublet structure at the L_2 edge, characteristic of a high-spin Ni^{2+} ion in O_h symmetry, as expected for such a Cr_7Ni-*bu* ring.[46,47] Since the spectra of the powders perfectly reproduce those of the ML, we conclude that the deposition by sublimation onto the gold surface does not affect the

valence electronic structure of the Cr and Ni ions: namely, oxidation state, local environment, and crystal-field intensity at the Cr and Ni sites.

Information on the intramolecular interactions can be extracted from the study of the sign of the dichroic signal. Indeed, when an external magnetic field is applied, a competition arises between the antiferromagnetic coupling between nearest-neighboring ions and the Zeeman interaction tending to align the magnetic moments along the field direction. The sign and intensities of the XMCD spectra of the ML (Figure 6, bottom panel) overlap those of the powders. The negative dichroic signal at the Cr L_3 edge and the positive one at the L_2 edge imply that the total magnetic moment of Cr ions is parallel to the applied magnetic field (*H*). The opposite behavior was observed for Ni for both powders and MLs at 7 K, implying that the magnetic moment is antiparallel to *H*, as expected. These results show that the deposition of Cr_7Ni by sublimation preserves the magnetic properties of these molecular rings.

CONCLUSIONS

Molecular Cr_7Ni derivatives are shown to be suitable for sublimation in UHV conditions. The different assembling of pristine Cr_7Ni-*bu*, as compared to that of Cr_7Ni-*thibu* functionalized with thiol, evidences the interplay between the intermolecular interaction and that with the gold substrate (Cu(110) and HOPG were also considered for comparison). The experimental observations are fully supported by DFT calculations in terms of a significantly different diffusion energy barrier between sulfured and pristine molecules. These finding are corroborated by XMCD spectra taken at low temperature that demonstrate that the magnetic properties of UHV deposited rings are unchanged with respect to those of the same molecules on bulk.

The capability of assembling complex functional MnM opens the way to study and exploit ordered 2D *ensembles*, which is a fundamental step for the realization of high-density memories, scalable devices for information processing, or hybrid architectures for qubit encoding or storage. Moreover, metamaterials made of ordered monolayers of functional MnM can also be envisaged, a path not yet explored but certainly with interesting potentialities.

METHODS

Chemical Synthesis. All reagents were from Aldrich and were used as received.

1. $\{[(CH_3)_2CHCH_2]_2NH_2\}\{Cr_7NiF_8[O_2CC(CH_3)_3]_{16}\}$, Cr_7Ni-*bu*, was prepared by adapting the method given in ref 38. Heating with stirring in a Teflon flask at 160 °C for 16 h of pivalic acid, $(CH_3)_3CCOOH$ (20 g, 196 mmol), disobutylamine, $[(CH_3)_2CHCH_2]_2NH$ (1.5 g, 11.6 mmol), chromium(III) fluoride tetrahydrate, $CrF_3 \cdot 0.4H_2O$ (5.0 g, 27.6 mmol), and nickel(II) carbonate hydroxide tetrahydrate, $2NiCO_3 \cdot 3Ni(OH)_2 \cdot 4H_2O$ (0.6 g, 1.0 mmol), resulted in a green microcrystalline product. After this, the flask was cooled to room temperature, and acetone (30 mL) was then added with stirring, to complete the precipitation of the final compound. It was collected by filtration, washed copiously with acetone, and then dissolved in pentane (60 mL). The pentane solution was filtered, and the filtrate was diluted with acetone (60 mL). Concentration of the solution by evaporation at room temperature produces large green crystals. Yield: 8.5 g (92.75% based on Cr). Anal. Calcd (%) for $C_{88}H_{164}Cr_7F_8NNiO_{32}$: Cr 15.67; Ni 2.53; C45.50; H 7.12; N 0.60. Found: Cr 15.58; Ni 2.55; C 45.0;H 7.14; N 0.58. Electrospray-MS (THF) *m/z*: +2345 $[M + Na]^+$.

X-ray quality crystals were obtained by crystallization of Cr_7Ni-*bu* from ethylacetate.

2. $\{HSCH_2CH_2NH_2CH_2CH_2CH_2CH_3\}\{Cr_7NiF_8[O_2CC(CH_3)_3]_{16}\}$, Cr_7Ni-*thiobu*, was prepared by the method given in ref 39.

UHV Experiments. The surface of Au(111) single crystals was prepared by repeated sputtering (Ar^+) and annealing (430 °C) cycles until the herringbone $22\times\sqrt{3}$ reconstruction was observed (by STM or LEED). Powder samples of Cr_7Ni-*bu* and Cr_7Ni-*thiobu* were deposited, after purification, by sublimation through resistive heating of a crucible realized by means of a borosilicate glass vial, positioning the substrate in front of a crucible at a distance of 10 cm, and using a type K thermocouple for temperature readout. Depositions were performed in the temperature range 180−230 °C and pressure of 2×10^{-8} mbar, while the amount of deposited molecules was determined by XPS. Surface preparation, deposition, and analysis were carried out in parallel in two ultrahigh vacuum UHV chambers, one for STM and one for spectroscopic experiments. The calibration of the evaporator of the STM chamber was performed by *ex situ* XPS measurements. The deposition rate used in STM experiments was twice that of the XPS experiments. It follows that 1 ML is obtaind with exposures of 60 and 120 min in the case of STM and XPS systems, respectively.

STM experiments were carried out at room temperature in UHV with electrochemically etched W tips by means of an Omicron VT-SPM microscope working in constant-current mode.

XPS measurements were performed in UHV using an Omicron hemispherical analyzer (EA125) and a nonmonochromatized Mg Kα X-ray source ($h\nu = 1253.6$ eV) with an overall energy resolution of 1.0 eV. The S-2p fitting procedure has been performed using spin−orbit-split doublet components (Voigt functions), with the following parameters: spin−orbit splitting of 1.2 eV, branching ratio of 0.5, Lorentzian width of 574 meV, and Gaussian width of 2400 meV for all components.

XMCD experiments were carried out at the ID8 beamline of the European Synchrotron Radiation Facility in Grenoble, France. The lowest sample temperature was about 7 K, and the base pressure of the experimental chamber was 1.0×10^{-9} mbar during sublimation and 1.0×10^{-10} mbar during measurements. The photon source was an Apple II undulator that delivers a high flux of polarized light. We paid much attention to avoid any sample degradation induced by radiation exposure, working with very low flux (below 10^{12} photons/s) and by strictly monitoring XAS spectra throughout all the experiments for detecting even the smallest traces of sample damaging. XMCD measurements at the Cr and Ni $L_{2,3}$ edges were performed in total electron yield mode using circularly polarized light with about 100% polarization rate and with an external magnetic field $\mu_0 H = 5$ T applied perpendicularly to the sample surface and parallel to the incident photon beam. The dichroic spectrum is the difference between the XAS spectra taken with the helicity of the incident photon antiparallel ($\sigma^{\uparrow\downarrow}$) and parallel

($\sigma^{\uparrow\downarrow}$) to the sample magnetization. In order to minimize the effects of field inhomogeneity, we carried out measurements by switching both the helicity and the applied field.

Acknowledgment. This work has been partially supported by FP7-ICT FET Open "MolSpinQIP" project, contract no. 211284, by the EPSRC (UK), and by MIUR-PRIN projects, contracts no. 2008PARRTS and no. 2008NX9Y7. We acknowledge the CINECA supercomputing center for the availability of high-performance computing resources and support. R.E.P.W. thanks the Royal Society for a Wolfson Merit Award. We acknowledge the European Synchrotron Radiation Facility for provision of synchrotron radiation facilities.

Supporting Information Available: Chemical synthesis, X-ray spectroscopy, infrared spectrometry, magnetic susceptibility, further STM and XPS data, and theoretical results. This material is available free of charge *via* the Internet at http://pubs.acs.org.

REFERENCES AND NOTES

1. Barth, J. V.; Costantini, G.; Kern, K. Engineering Atomic and Molecular Nanostructures at Surfaces. *Nature* **2005**, *437*, 671–679.
2. Joachim, C.; Gimzewski, J. K.; Aviram, A. Electronics Using Hybrid-Molecular and Mono-Molecular Devices. *Nature* **2000**, *408*, 541–548.
3. Bogani, L.; Wernsdorfer, W. Molecular Spintronics Using Single-Molecule Magnets. *Nat. Mater.* **2008**, *7*, 179–186.
4. Foster, J. S.; Frommer, J. E. Imaging of Liquid Crystals Using a Tunnelling Microscope. *Nature* **1988**, *333*, 542–545.
5. Schreiber, F. Self-Assembled Monolayers: from `Simple' Model Systems to Biofunctionalized Interfaces. *J. Phys.: Condens. Matter* **2004**, *16*, R881–R900.
6. Jung, T. A.; Schlittler, R. R.; Gimzewski, J. K. Conformational Identification of Individual Adsorbed Molecules with the STM. *Nature* **1997**, *386*, 696–698.
7. Otsuki, J. STM Studies on Porphyrins. *Coord. Chem. Rev.* **2010**, *254*, 2311–2341.
8. Ma, H.; Ou Yang, L.-Y.; Pan, N.; Yau, S.-L.; Jiang, J.; Itaya, K. Ordered Molecular Assemblies of Substituted Bis-(phthalocyaninato) Rare Earth Complexes on Au(111): In Situ Scanning Tunneling Microscopy and Electrochemical Studies. *Langmuir* **2006**, *22*, 2105–2111.
9. Gomez-Segura, J.; Dez-Perez, I.; Ishikawa, N.; Nakano, M.; Veciana, J.; Ruiz-Molina, D. 2-D Self-Assembly of the bis-(phthalocyaninato)terbium(III) Single-Molecule Magnet Studied by Scanning Tunneling Microscopy. *Chem. Commun.* **2006**, 2866–2868.
10. Elemans, J. A. A. W.; Lei, S.; De Feyter, S. Molecular and Supramolecular Networks on Surfaces: From Two-Dimensional Crystal Engineering to Reactivity. *Angew. Chem., Int. Ed.* **2009**, *48*, 7298–7332.
11. Love, J. C.; Estroff, L. A.; Kriebel, J. K.; Nuzzo, R. G.; Whitesides, G. M. Self-Assembled Monolayers of Thiolates on Metals as a Form of Nanotechnology. *Chem. Rev.* **2005**, *105*, 1103–1169.
12. Gatteschi, D., Villain, J., Sessoli, R. *Molecular Nanomagnets*; Oxford Univ. Press, 2006.
13. Carretta, S.; Santini, P.; Amoretti, G.; Guidi, T.; Copley, J. R. D.; Qiu, Y.; Caciuffo, R.; Timco, G. A.; Winpenny, R. E. P. Quantum Oscillations of the Total Spin in a Heterometallic Antiferromagnetic Ring: Evidence from Neutron Spectroscopy. *Phys. Rev. Lett.* **2007**, *98*, 167401.
14. Ardavan, A.; Rival, O.; Morton, J. J. L.; Blundell, S. J.; Tyryshkin, A. M.; Timco, G. A.; Winpenny, R. E. P. Will Spin-Relaxation Times in Molecular Magnets Permit Quantum Information Processing? *Phys. Rev. Lett.* **2007**, *98*, 057201.
15. Troiani, F.; Ghirri, A.; Affronte, M.; Carretta, S.; Santini, P.; Amoretti, G.; Piligkos, S.; Timco, G. A.; Winpenny, R. E. P. Molecular Engineering of Antiferromagnetic Rings for Quantum Computation. *Phys. Rev. Lett.* **2005**, *94*, 207208.
16. Timco, G. A.; Carretta, S.; Troiani, F.; Tuna, F.; Pritchard, R. J.; Muryn, C. A.; McInnes, E. J. L.; Ghirri, A.; Candini, A.; Santini, P.; *et al.* Engineering the Coupling between Molecular Spin Qubits by Coordination Chemistry. *Nat. Nanotechnol.* **2009**, *4*, 173–178.
17. Candini, A.; Lorusso, G.; Troiani, F.; Ghirri, A.; Carretta, S.; Santini, P.; Amoretti, G.; Muryn, C.; Tuna, F.; Timco, G.; McInnes, E. J. L.; Winpenny, R. E. P.; Wernsdorfer, W.; Affronte, M. Entanglement in Supramolecular Spin Systems of Two Weakly Coupled Antiferromagnetic Rings (Purple-Cr_7Ni). *Phys. Rev. Lett.* **2010**, *104*, 037203.
18. Troiani, F.; Bellini, V.; Candini, A.; Lorusso, G.; Affronte, M. Spin Entanglement in Supramolecular Structures. *Nanotechnology* **2010**, *21*, 274009.
19. Gomez-Segura, J.; Veciana, J.; Ruiz-Molina, D. Advances on the Nanostructuration of Magnetic Molecules on Surfaces: the Case of Single-Molecule Magnets (SMM). *Chem. Commun.* **2007**, 3699–3707.
20. Gatteschi, D.; Cornia, A.; Mannini, M.; Sessoli, R. Organizing and Addressing Magnetic Molecules. *Inorg. Chem.* **2009**, *48*, 3408–3419.
21. Ruiz-Molina, D.; Mas-Torrent, M.; Gomez, J.; Balana, A. I.; Domingo, N.; Tejada, J.; Martnez, M. T.; Rovira, C.; Veciana, J. Isolated Single-Molecule Magnets on the Surface of a Polymeric Thin Film. *Adv. Mater.* **2003**, *15*, 42–45.
22. Cornia, A.; Fabretti, A. C.; Pacchioni, M.; Zobbi, L.; Bonacchi, D.; Caneschi, A.; Gatteschi, D.; Biagi, R.; Del Pennino, U.; De Renzi, V.; *et al.* Direct Observation of Single−Molecule Magnets Organized on Gold Surfaces. *Angew. Chem., Int. Ed.* **2003**, *42*, 1645–1648.
23. Coronado, E.; Forment-Aliaga, A.; Romero, F. M.; Corradini, V.; Biagi, R.; de Renzi, V.; Gambardella, A.; del Pennino, U. Isolated Mn12 Single-Molecule Magnets Grafted on Gold Surfaces *via* Electrostatic Interactions. *Inorg. Chem.* **2005**, *44*, 7693–7695.
24. Corradini, V.; Ghirri, A.; del Pennino, U.; Biagi, R.; Milway, V. A.; Timco, G.; Tuna, F.; Winpenny, R. E. P.; Affronte, M. Grafting Molecular Cr_7Ni Rings on a Gold Surface. *Dalton Trans.* **2010**, *39*, 4928–4936.
25. Fleury, B.; Volatron, F.; Catala, L.; Brinzei, D.; Rivière, E.; Huc, V.; David, C.; Miserque, F.; Rogez, G.; Baraton, L.; *et al.* A New Approach to Grafting a Monolayer of Oriented Mn_{12} Nanomagnets on Silicon. *Chem. Commun.* **2005**, 2020–2022.
26. Ghirri, A.; Corradini, V.; Cervetti, C.; Candini, A.; del Pennino, U.; Timco, G.; Pritchard, R. J.; Muryn, C. A.; Winpenny, R. E. P.; Affronte, M. Deposition of Functionalized Cr_7Ni Molecular Rings on Graphite from the Liquid Phase. *Adv. Funct. Mater.* **2010**, *20*, 1552–1560.
27. Mannini, M.; Pineider, F.; Danieli, C.; Totti, F.; Sorace, L.; Sainctavit, Ph.; Arrio, M.-A.; Otero, E.; Joly, L.; Cezar, J. C.; *et al.* Quantum Tunnelling of the Magnetization in a Monolayer of Oriented Single-Molecule Magnets. *Nature* **2010**, *468*, 417–422.
28. Corradini, V.; Moro, F.; Biagi, R.; De Renzi, V.; del Pennino, U.; Bellini, V.; Carretta, S.; Santini, P.; Milway, V. A.; Timco, G. M.; *et al.* Successful Grafting of Isolated Molecular Cr_7Ni Rings on Au(111) Surface. *Phys. Rev. B* **2009**, *79*, 144419.
29. Margheriti, L.; Mannini, M.; Sorace, L.; Gorini, L.; Gatteschi, D.; Caneschi, A.; Chiappe, D.; Moroni, R.; Buatier de Mongeot, F.; Cornia, A.; *et al.* Thermal Deposition of Intact Tetrairon(III) Single-Molecule Magnets in High-Vacuum Conditions. *Small* **2009**, *5*, 1460–1466.
30. Margheriti, L.; Chiappe, D.; Mannini, M.; Car, P.; Sainctavit, P.; Arrio, M.-A.; de Mongeot, F. B.; Cezar, J. C.; Piras, F. M.; Magnani, A.; *et al.* X-Ray Detected Magnetic Hysteresis of Thermally Evaporated Terbium Double-Decker Oriented Films. *Adv. Mater.* **2010**, *22*, 5488–5493.
31. Stepanow, S.; Honolka, J.; Gambardella, P.; Vitali, L.; Abdura-Khmanova, N.; Tseng, T.-C.; Rauschenbach, S.; Tait, S. L.; Sessi, V.; Klyatskaya, S.; *et al.* Spin and Orbital Magnetic Moment Anisotropies of Monodispersed Bis(phthalocyaninato)terbium on a Copper Surface. *J. Am. Chem. Soc.* **2010**, *132*, 11900–11901.
32. Rancan, M.; Sedona, F.; Di Marino, M.; Armelao, L.; Sandi, M. Chromium Wheels *Quasi*-Hexagonal 2D Assembling by Direct UHV Sublimation. *Chem. Commun.* **2011**, *47*, 5744–5746.

33. Saywell, A.; Magnano, G.; Satterley, C. J.; Perdigão, L. M. A.; Britton, A. J.; Taleb, N.; Giménez-López, M. C.; Champness, N. R.; O'Shea, J. N.; Beton, P. H. Self-Assembled Aggregates Formed by Single Molecule Magnets on a Gold Surface. *Nat. Commun.* **2010**, *1*, 75.
34. Corradini, V.; Cervetti, C.; Ghirri, A.; Biagi, R.; del Pennino, U.; Timco, G. A.; Winpenny, R. E. P.; Affronte, M. Oxo-Centered Carboxylate-Bridged Trinuclear Complexes Deposited on Au(111) by a Mass-Selective Electrospray. *New J. Chem.* **2011**, *35*, 1683–1689.
35. Mura, M.; Gulans, A.; Thonhauser, T.; Kantorovich, L. Role of van der Waals Interaction in Forming Molecule-Metal Junctions: Flat Organic Molecules on the Au(111) Surface. *Phys. Chem. Chem. Phys.* **2010**, *12*, 4759–4767.
36. Maksymovych, P.; Voznyy, O.; Dougherty, D. B.; Sorescu, D. C.; Yates, J. T., Jr. Gold Adatom as a Key Structural Component in Self-Assembled Monolayers of Organosulfur Molecules on Au(1 1 1). *Prog. Surf. Sci.* **2010**, *85*, 206–240.
37. Iljina, E.; Korjeva, A.; Kuzmina, N.; Troyanov, S.; Dunaeva, K.; Martynenko, L. The Volatile Pivalates of Y, Ba and Cu as Prospective Precursors for Metal-Organic Chemical Vapour Deposition. *Mater. Sci. Eng.: B* **1993**, *18*, 234–236.
38. Larsen, F. K.; McInnes, E. J. L.; ElMkami, H.; Overgaard, J.; Piligkos, S.; Rajaraman, G.; Rentscheler, E.; Smith, A. A.; Smith, G. M.; Boothe, V.; *et al*. Synthesis and Characterization of Heterometallic $\{Cr_7M\}$ Wheels. *Angew. Chem., Int. Ed.* **2003**, *42*, 101–105.
39. Corradini, V.; Biagi, R.; del Pennino, U.; De Renzi, V.; Gambardella, A.; Affronte, M.; Muryn, C. A.; Timco, G. A.; Winpenny, R. E. P. Isolated Heterometallic Cr_7Ni Rings Grafted on Au(111) Surface. *Inorg. Chem.* **2007**, *46*, 4937–4943.
40. Castner, D. G.; Hinds, K.; Grainger, D. W. X-Ray Photoelectron Spectroscopy Sulfur 2p Study of Organic Thiol and Disulfide Interactions with Gold Surfaces. *Langmuir* **1996**, *12*, 5083–5086.
41. Ishida, T.; Choi, N.; Mizutani, W.; Tokumoto, H.; Kojima, I.; Azehara, H.; Hokari, H.; Akiba, U.; Fujihira, M. High-Resolution X-ray Photoelectron Spectra of Organosulfur Monolayers on Au(111): S(2p) Spectral Dependence on Molecular Species. *Langmuir* **1999**, *15*, 6799.
42. Ishida, T.; Hara, M.; Kojima, I.; Tsuneda, S.; Nishida, N.; Sasabe, H.; Knoll, W. High Resolution X-Ray Photoelectron Spectroscopy Measurements of Octadecanethiol Self-Assembled Monolayers on Au(111). *Langmuir* **1998**, *14*, 2092–2096.
43. Poirier, G. E. Mechanism of Formation of Au Vacancy Islands in Alkanethiol Monolayers on Au(111). *Langmuir* **1997**, *13*, 2019–2026.
44. Yang, G.; Liu, G.-Y. New Insights for Self-Assembled Monolayers of Organothiols on Au(111) Revealed by Scanning Tunneling Microscopy. *J. Phys. Chem. B* **2003**, *107*, 8746–8759.
45. Mazzarello, R.; Cossaro, A.; Verdini, A.; Rousseau, R.; Casalis, L.; Danisman, M. F.; Floreano, L.; Scandolo, S.; Morgante, A.; Scoles, G. Structure of a CH3 S Monolayer on Au(111) Solved by the Interplay between Molecular Dynamics Calculations and Diffraction Measurements. *Phys. Rev. Lett.* **2007**, *98*, 016102.
46. Corradini, V.; Moro, F.; Biagi, R.; del Pennino, U.; De Renzi, V.; Carretta, S.; Santini, P.; Affronte, M.; Cezar, J. C.; Timco, G. A.; *et al*. X-ray Magnetic Circular Dichroism Investigation of Spin and Orbital Moments in Cr_8 and Cr_7Ni Antiferromagnetic Rings. *Phys. Rev. B* **2008**, *77*, 014402.
47. Ghirri, A.; Lorusso, G.; Moro, F.; Troiani, F.; Corradini, V.; Muryn, C.; Tuna, F.; Timco, G. A.; Winpenny, R. E. P.; Affronte, M. Probing Edge Magnetization in Antiferromagnetic Spin Segments. *Phys. Rev. B* **2009**, *79*, 224430.